An Effective Method to Enhance Adsorption Capacity and Mesoporosity of Activated Carbon by Pre-Pyrolysis and Chemical Activation Procedures

Tzong-Horng Liou,[a,b,*] Pie Ying Wang,[a] and Yuan Hao Liou [a]

Activated carbons with large adsorption capacity and high mesopore fraction were obtained from rice straw by a combination of pre-pyrolysis and NaOH activation procedures. The experiments varied the pre-pyrolysis procedure, impregnation ratio of activating agent, and activation temperature. Samples were examined by inductively coupled plasma-mass spectrometry (ICP-MS), X-ray diffractometry (XRD), field-emission scanning-electronic microscopy (FE-SEM), thermogravimetric analysis (TGA), and N_2-adsorption analysis. The surface area and pore characteristics of the activated carbons were investigated by the Brunauer, Emmett, Teller (BET) method, Dubinin-Raduch (DR) model, and the *t*-plot method. The surface area, pore volume, and iodine adsorption capacity of the samples increased with increasing activation temperature and the impregnation ratio of the activating agent. A maximum surface area of 2093 m^2/g was obtained at the activation temperature of 900 °C. The pore structure in the one-stage activation procedure was mainly microporous. Two-stage activation procedure efficiently enhanced mesopore volume, and therefore further increased the adsorption capacity of activated carbons. NaOH acted as both the activating agent in the reaction and as the cleaner to remove the ash. The results of this experiment will be useful in developing resource recovery systems from agricultural biomass.

Keywords: Rice straw; Activated carbon; Sodium hydroxide; Pre-pyrolysis, Mesoporosity

*Contact information: a: Department of Chemical Engineering and b: Battery Research Center of Green Energy, Ming Chi University of Technology, 84 Gungjuan Rd., Taishan, New Taipei City 24301, Taiwan; * Corresponding author: thliou@mail.mcut.edu.tw*

INTRODUCTION

Activated carbon (AC) is a high-porosity material with a large adsorption capacity, and it is widely used as an adsorbent for filtration and purification (Kim and Pui 2015; El-Naggar *et al.* 2016). Recent environmental quality requirements have increased the demand for AC. According to the IUPAC classification, the micropores are less than 2 nm wide, mesopores are 2 to 50 nm wide, and macropores are more than 50 nm wide. The structure of AC synthesized using traditional alkali hydroxide activation (NaOH, KOH) is mainly constituted by microporous (Yang *et al.* 2015). However, larger pores provide more favorable mass transfer kinetics (Liou 2010). Carbon materials obtained from alkali hydroxide activation and pre-pyrolysis have high mesoporous volume and large adsorption capacity. The high surface area of AC and its balance between micro- and mesoporosity provide an appropriate medium for energy storage (CH_4 and H_2) and CO_2 sorption (Liu *et al.* 2014; Sethia and Sayari 2015).

Rice straw is a by-product of the rice milling industry. Its main components based on the weight percentage concentration are cellulose (54.5 wt%), pentosans (13.2 wt%), lignin

(18.9 wt%), and ash (Basta *et al.* 2011). Approximately 15 to 20 wt% of the ash is obtained from burning rice straw in air. The ash contains 75 wt% silica (Tsai *et al.* 2006). Rice straw accounts for about 50% of the total weight of rice plants (Putum *et al.* 2004). 500 million tons of rice are produced annually (Chuah et al. 2005). Rice straw is bulky, and only a few parts are used as fuel. This waste creates a disposal problem, with the amount increasing each year. Rice straw has been suggested for the use of raw materials such as pulp, construction materials, and precursors for energy production. However, the applications of rice straw are limited due to its high silica content. AC powder with high porosity and large surface area can be obtained by activating rice straw in an inert atmosphere. Because rice straw is also inexpensive and widely available, it is a very good candidate to prepare AC.

To obtain mesoporous AC powder, traditional practices use carbon precursors in the presence of transition metals or hydrothermal pre-treatments, followed by an activation process (Jain *et al.* 2015). Tseng (2006) studied the NaOH activation of corn cob and found that the mesoporous volume of the AC was significantly enhanced by using a concentrated NaOH solution. Compared with KOH activation, the high dosage of NaOH kept on etching the carbon and turned the micropores into mesopores. Therefore, NaOH activation suitably controls the mesopore specific volume of the AC. Zabaniotou *et al.* (2008) produced AC using olive kernels with simultaneous pyrolysis and activation by KOH. They found that the produced carbons were composed of micropores at the early stages of activation and both micropores and mesopores at the later stages.

This study treated rice straw by a combination of pre-pyrolysis and NaOH activation procedures, in order to obtain AC with high-mesoporosity and large adsorption capacity. The physical and chemical characteristics of the carbon materials were analyzed through various techniques such as inductively coupled plasma-mass spectrometer (ICP-MS), field-emission scanning-electronic microscopy (FE-SEM), X-ray diffractometry (XRD), thermogravimetric analysis (TGA), and N_2 adsorption analysis. The surface area and pore characteristics of the samples were analyzed using the Brunauer, Emmett, Teller (BET) method, the Dubinin-Raduch (DR) model, and the *t*-plot method.

EXPERIMENTAL

Materials Used and Sample Preparation

Raw dried rice straw (DRS) obtained from a rice paddy in Taoyuan, Taiwan was used. It was washed thoroughly with distilled water to remove adhering soil and clay and then oven-dried at 100 °C for 24 h. Laboratory grade NaOH was purchased from Merck (Darmstadt, Germany). As determined by ultimate analysis, the rice straw contained carbon (36.52 wt%), hydrogen (6.23 wt%), and nitrogen (0.55 wt%).

AC was prepared from rice straw using both the one- and two-stage activation procedures. In the one-stage activation procedure, the DRS was impregnated with NaOH and water at impregnation ratios of 1-3. The impregnation ratio (R) was defined as the mass ratio of activating agent to DRS. The impregnated sample was set in a sand bath to remove excess water and placed into a stainless steel container. Highly pure nitrogen gas (99.995%, San-Fu Chem. Co., Taipei, Taiwan) was used as the purge gas. The reactor was inserted into a furnace for 1 h at 700 ^{o}C.

In the two-stage activation procedure, the DRS was first pyrolyzed between 300 to 800 °C for 1 h in the presence of nitrogen. The impregnation method and heating procedure were the same as in the one-stage procedure. In a typical procedure for impregnation ratio

of 2, 2 g of NaOH was dissolved in water. The 1 g of pre-pyrolyzed rice straw was mixed with the NaOH solution, and then heated at a specified temperature.

Finally, the samples were washed thoroughly with distilled water to remove residual chemicals. The washed samples were dried at 105 ºC for 24 h, and then ground and screened through a standard sieve of 325 mesh. The activated carbons have size between 38 and 45 μm.

Analysis of Surface Area and Pore Characteristics

The specific surface area, pore volume, and pore diameter of AC samples were determined using the N_2-adsorption analyzer (model ASAP 2010, Micrometric, Sarasota, FL, USA). The specific surface areas of the carbons were calculated by the BET method (Passe-Coutrin *et al.* 2008). The Dubinin-Raduskevich equation was applied to characterize the microporosity of the AC samples (Scherdel *et al.* 2010), as follows,

$$\ln(V_{ads}) = \ln(V_{DR}) - \left(\frac{R_{gas}T}{E_{DR}\beta}\right)^2 \cdot \left[\ln\left(\frac{P_o}{P}\right)\right]^2 \quad (1)$$

where R_{gas} is the gas constant (8.314 J/mol-K), T is the analysis temperature (K), β is the affinity coefficient (β = 0.33 for nitrogen), and E_{DR} is the interaction energy (J). V_{DR} represents the limiting micropore volume (cm^3) derived from the intercept in the linear region of the DR-plot ($\ln(V_{ads})$ *vs.* $\ln^2(P_o/P)$). The second tool, the *t*-plot method, was applied to distinguish between micropores and external surface area (Lépinay *et al.* 2015). The micropore volume ($V_{t\text{-}plot}$) and external surface area (S_{ext}) were determined from the intercept and slope, respectively, of the linear fit.

Analysis of Physical and Chemical Properties

Metallic impurities in the AC samples were determined using an inductively coupled plasma-mass spectrometer (model Agilent 7500ce, Agilent Technologies, Tokyo, Japan). The ACs were dissolved in a solution of HNO_3 and HF, and heated at 180 °C for 6 h. The amounts of metallic impurities in the solution were then determined with an ICP-MS. The crystalline structure of the reactant and product was examined by an X-ray diffractometer (model D-500, Siemens, Aubrey, TX, USA). The morphology of the reactant and product was obtained with a field-emission scanning-electron microscope (model ABT-150S, Topcon, Tokyo, Japan). The thermal characteristics of the rice straw impregnated with the activating agent were measured using a Perkin-Elmer TGA7 thermogravimetric analyzer (USA).

The adsorption tests of ACs were conducted using iodine adsorption capacity. Then 0.1 g of AC was placed in a flask containing a 35 mL of 0.1 N iodine solution, and shaken to maintain equilibrium for 24 h. After adsorption, the adsorbent was removed by filtration. The iodine adsorption capacity was determined from the titration of the 5 mL of filtrate with a 0.1 N sodium thiosulfate ($Na_2S_2O_3$) solution using 2.5 mL of starch as indicator.

RESULTS AND DISCUSSION

Analysis of Metallic Impurities of AC Samples

Table 1 shows that the Na, Mg, K, Ca, and Fe were present as major impurities. After alkali hydroxide activation, the ACs showed an obvious increase in Na species. For

one- and two-stage activation procedures, the total metallic impurities decreased with an increasing impregnation ratio of the activating agent. For the same impregnation ratio of the activating agent, the total metallic impurities in the carbon samples prepared from one-stage activation procedure was noticeably higher than that of the samples prepared from the two-stage activation procedure. The purity of ACs synthesized by one- and two-stage activation procedures was as high as 99.7 wt%.

Table 1. Metallic Ingredients in AC Samples

Impregnation Ratio	Metallic ingredients as oxides (ppm)									
	Na	Mg	P	K	Ca	Mn	Fe	Cu	Zn	Total
R = 1[a]	4625	937	ND	873	9201	147	152	ND	ND	15935
R = 2[a]	472	513	ND	612	1268	40	687	2083	1003	6678
R = 3[a]	364	308	ND	601	ND	111	372	654	302	2712
R = 1[b]	4793	1609	1426	287	619	496	1901	ND	ND	11131
R = 2[b]	1739	993	ND	577	1882	357	335	26	ND	5909
R = 3[b]	669	413	110	382	418	220	110	159	135	2616

[a] One-stage activation procedure; [b] two-stage activation procedure. ND, not detected.

Effect of Activation Procedure on the Adsorption Capacity

Figures 1(a) and (b) show that the minimum BET surface area and iodine adsorption capacity of 292 m^2/g and 120 mg/g occurred in the sample when the DRS was carbonized in N_2 without the addition of the chemical activating agent (R = 0). The increase of the surface area is due to the volatilization of organic matter during the carbonization of DRS. When the DRSs were treated with a one-stage activation procedure, the samples had BET surface areas that ranged from 950 to 1139 m^2/g and iodine adsorption capacities of 510 to 765 mg/g, which increased with an increasing impregnation ratio.

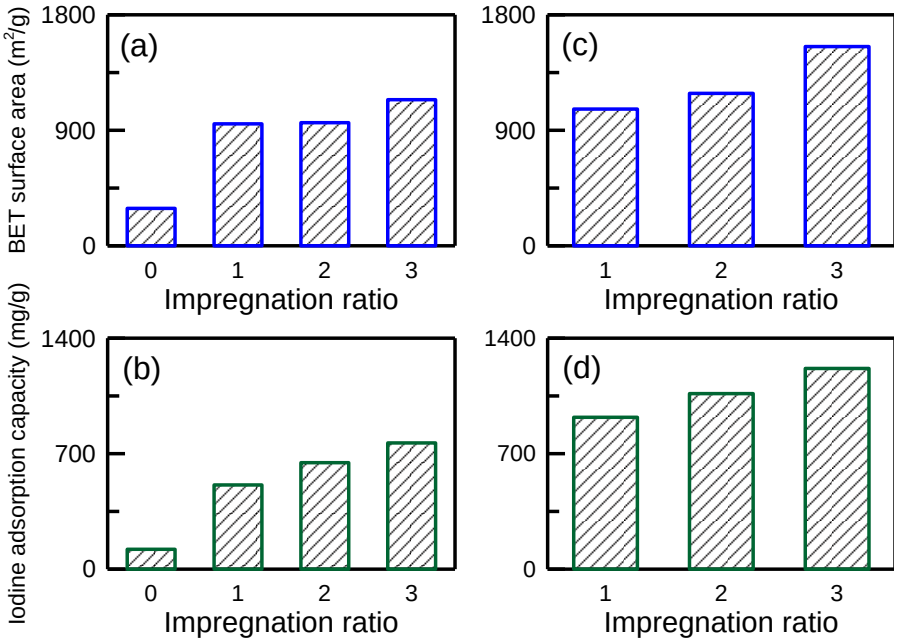

Fig. 1. Surface area (a and c) and iodine adsorption capacity (b and d) of ACs at various impregnation ratios, formed by one-stage activation (a and b) or two-stage activation (c and d)

Vilaplana-Ortego *et al.* (2009) reported the activation of isotropic petroleum pitch with KOH and concluded that the surface area of the samples increases with an increasing impregnation ratio of activating agent, which is consistent with the observations in this study. By increasing the activating agent, there is more contact area between DRS and NaOH, which enhances the activation reaction.

Figures 1(c) and (d) show that the surface areas ranged from 1066 to 1553 m^2/g, and iodine adsorption capacities were 920 to 1216 mg/g when the impregnation ratio of NaOH was increased from 1 to 3 for the two-stage activation procedure. The trend of surface area increasing with increasing impregnation ratio was the same as that of the one-stage activation procedure. However, the surface areas and iodine adsorption capacities in the two-stage activation procedure were obviously much higher than in the one-stage activation procedure.

Figures 2(a) and (b) show that the surface area and iodine adsorption capacity of AC reached their maximum value when the pre-pyrolysis temperature was 500 °C. The surface area was relatively small when the pre-pyrolysis temperature was 300 °C. This result may be due to carbonization occurring only at the DRS exterior. When the pre-pyrolysis temperature exceeded 500 °C, the surface area decreased slightly with increasing pre-pyrolysis temperature. Thus, violent gasification reactions may partially destroy the pore structure at high-pyrolysis temperature (Liou and Wu 2009).

At the same impregnation ratio, Figs. 2(c) and (d) show that the surface area increased as the activation temperature increased. The maximum BET surface area of 2093 m^2/g and iodine adsorption capacity of 1450 mg/g were observed at 900 °C. However, when the activation temperature was increased to 1000 °C, the carbon structure was destroyed due to the drastic gasification reaction, which suggests that the activation temperature is important for controlling the specific surface area.

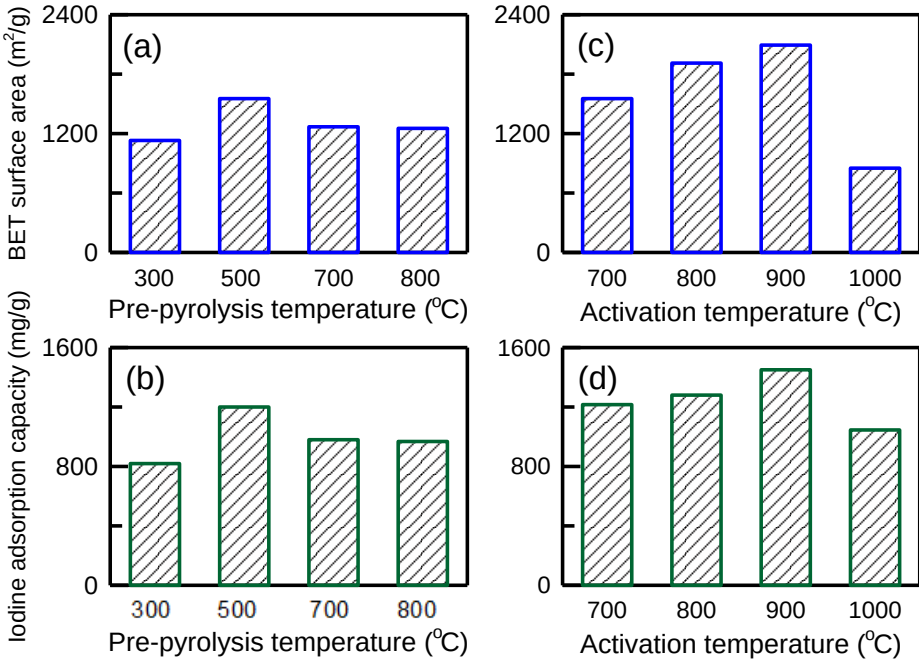

Fig. 2. Surface area (a and c) and iodine adsorption capacity (b and d) of ACs for two-stage activation procedure with (a and b) various pre-pyrolysis temperatures or (c and d) various activation temperatures

Analysis of Pore Structure

Figure 3(a) shows that the adsorption capacity increased noticeably as the impregnation ratio increased for the one-stage activation procedure. The shape of these isotherms did not display apparent hysteresis loops, indicating a characteristic Type I isotherm. The pore structure of the ACs for one-stage activation procedure was mainly microporous. Figure 3(b) shows a plot of the pore size distribution of the AC samples. These samples had no obvious peak, indicating that the pore diameters were smaller than 2 nm. In Fig. 3(c), the DR-plots with linear fits are shown. The intercept of the straight line increased slightly with a decreasing impregnation ratio of the activating agent. This result indicates that the micropore fraction (V_{DR}/V_t) decreased with increasing impregnation ratio (Table 2). Figure 3(d) shows the *t*-plot of the AC samples. There was a linear region extending through the *y*-axis, and the slope of the linear part was proportional to the external surface area (S_{ext}). The positive intercept indicated the presence of micropores (Hu and Srinivasan 1999), which agreed with the observed adsorption isotherms (Fig. 3(a)). The slope of the straight line increased with an increasing impregnation ratio, indicating the increase in external surface area (Table 2). The micropore volume ($V_{t\text{-plot}}$) and micropore fraction ($V_{t\text{-plot}}/V_t$) decreased with an increasing impregnation ratio, which was consistent with the DR-plots (V_{DR}/V_t). The micropore fraction was the lowest at an impregnation ratio of 3. Micropores may merge during activation, forming mesopores or macropores.

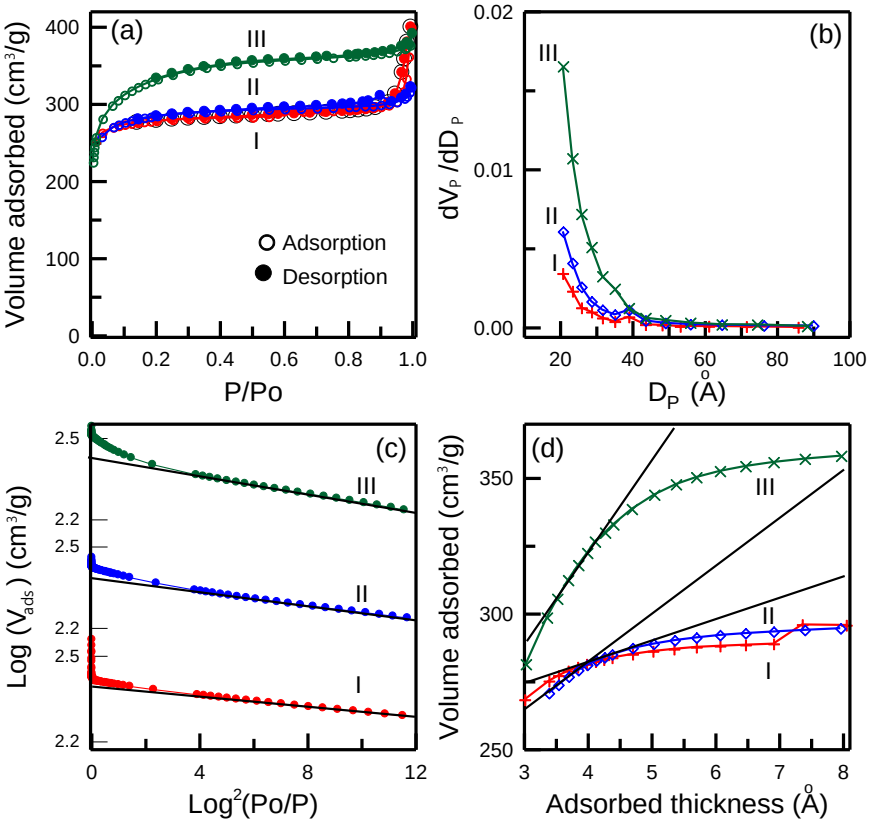

Fig. 3. (a) Adsorption-desorption isotherm, (b) differential pore size distribution, (c) DR-plot, and (d) t-plot of samples activated at 700 °C for the one-stage activation procedure (I R=1, II R=2, and III R=3; P/P_o is the relative pressure; D_p is the pore size)

Table 2. Analysis of Pore Characteristics at Various Impregnation Ratios for One-Stage Activation [a]

R	S_{BET} (m^2/g)	V_t (cm^3/g)	DR-plot		t-plot			
			V_{DR} (cm^3/g)	V_{DR}/V_t (%)	S_{ext} (m^2/g)	S_{mic} (m^2/g)	$V_{t\text{-plot}}$ (cm^3/g)	$V_{t\text{-plot}}/V_t$ (%)
0	292	--	--	--	--	--	--	--
1	951	0.498	0.392	78.71	105	846	0.393	78.92
2	960	0.506	0.386	76.28	178	782	0.363	71.74
3	1139	0.576	0.421	73.09	435	704	0.354	61.46

S_{BET} = BET surface area, V_t = total pore volume, V_{DR} = micropore volume by DR-plot method, S_{ext} = external surface area, $V_{t\text{-plot}}$ = micropore volume by *t*-plot method.
[a] Samples were impregnated with NaOH and an activation temperature of 700 °C.

Figure 4 shows the pore analysis for ACs obtained using the two-stage activation procedure at various impregnation ratios. At the low relative pressure of Fig. 4(a), the three isotherms displayed an abrupt increase in adsorbed volume, which was due to the formation of microporous structures (Liou 2010). When adsorption increased markedly at a P/P_o above 0.4, these samples showed Type IV hysteresis loops (Liou and Lai 2012). This effect may result from capillary condensation in the mesopores. Samples from the two-stage procedure had both micropores and mesopores. When the impregnation ratio was 3, the maximum adsorption capacity was observed. The total pore volume of the AC increased with increasing impregnation ratio (Table 3). Figure 4(b) shows the pore size distribution; the average pore diameters were 3 to 5 nm, indicating mesopores.

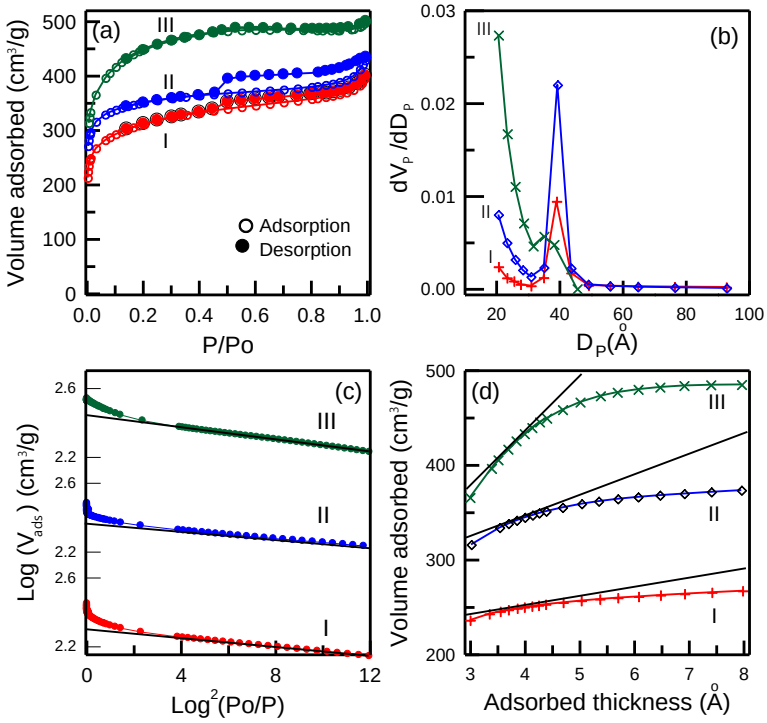

Fig. 4. (a) Adsorption-desorption isotherm, (b) differential pore size distribution, (c) DR-plot, and (d) t-plot of samples activated at 700 °C for the two-stage activation procedure (I *R*=1, II *R*=2, and III *R*=3; P/P_o is the relative pressure; D_p is the pore size)

Figure 4(c) shows the DR-plots of the AC samples. The maximum microporosity occurred at the impregnation ratio of 2 (Table 3). The same trend was observed in the *t*-plot curves (Fig. 4(d)). However, the impregnation ratio of 2 resulted in the minimum external surface area (S_{ext}). Comparing Figs. 3 and 4, the samples for the two-stage activation procedure showed a larger nitrogen adsorption capacity than those from the one-stage activation procedure. Hu and Srinivasan (1999) performed reactions with coconut shell and KOH and showed that ACs obtained by pre-heating at 600 °C showed higher adsorption capacity than those pre-heated at 110 °C, which is consistent with the present observation. However, the AC obtained from the two-stage activation procedure revealed a higher mesopore fraction. Thus, the combination of pre-pyrolysis and chemical activation effectively enhanced the mesoporosity and adsorption capacity of ACs.

The nitrogen adsorption capacities in Fig. 5(a) increased with increasing activation temperature from 700 to 900 °C for two-stage activation. The three isotherms displayed broad knees, which indicated that microporous and mesoporous structures developed noticeably in the samples. When the activation temperature was 1000 °C, the sample had the lowest nitrogen adsorption capacity. The carbon structure at 1000 °C may be destroyed by gasification reactions (Liou and Wu 2009). The maximum pore volume of 1.00 cm^3/g was observed at 900 °C (Table 4). Figure 5(b) shows that the average pore diameter of the ACs was 3 to 5 nm and increased with increasing activation temperature. The DR-plots of AC with a reaction temperature from 700 to 1000 °C are shown in Fig. 5(c). The samples at activation temperature between 700 and 1000 °C revealed a high proportion of mesoporosity (Table 4). The mesopore fraction was between 42 and 48% (based on 100% minus V_{DR}/V_t). Figure 5(d) shows the *t*-plots of the AC samples. When the activation temperatures were smaller than 900 °C, the slope of the straight line of the samples increased with increasing activation temperature. Table 4 shows that the external surface area (S_{ext}) increased with increasing activation temperature from 700 to 900 °C. When the activation temperature was 1000 °C, the external surface area was the lowest. It was hypothesized that the external surface area decreased by collapse of pore structures after thermal degradation of the pore walls.

Table 3. Analysis of Pore Characteristics at Various Impregnation Ratios for Two-Stage Activation [a]

R	S_{BET} (m^2/g)	V_t (cm^3/g)	DR-plot		t-plot			
			V_{DR} (cm^3/g)	V_{DR}/V_t (%)	S_{ext} (m^2/g)	S_{mic} (m^2/g)	$V_{t\text{-}plot}$ (cm^3/g)	$V_{t\text{-}plot}/V_t$ (%)
1	1066	0.592	0.317	53.55	406	660	0.305	51.52
2	1188	0.639	0.407	63.69	286	902	0.418	65.41
3	1553	0.759	0.391	51.52	709	844	0.385	50.72

S_{BET} = BET surface area, V_t = total pore volume, V_{DR} = micropore volume by DR-plot method, S_{ext} = external surface area, $V_{t\text{-}plot}$ = micropore volume by *t*-plot method.
[a] Samples were impregnated with NaOH, pre-pyrolysis temperature of 500 °C, and activation temperature of 700 °C.

In the literature, other bioresources such as macadamia nut shell, guava seed, and Euphorbia rigida have been reported to make AC materials by using NaOH activation (Martins *et al.* 2015; Pezoti *et al.* 2016; Kılıç *et al.* 2012). The mesopore ratio, surface area and pore volume of ACs range from 15.0 to 21.8 %, 396 to 2574 m^2/g, and 0.202 to 1.260 cm^3/g, respectively. The surface area and pore volume values of present work (1553 to

2093 m^2/g and 0.759 to 1.001 cm^3/g) are similar to those in the literature, but the mesopore ratio of present work (42 to 48%) was much higher than those of the literature.

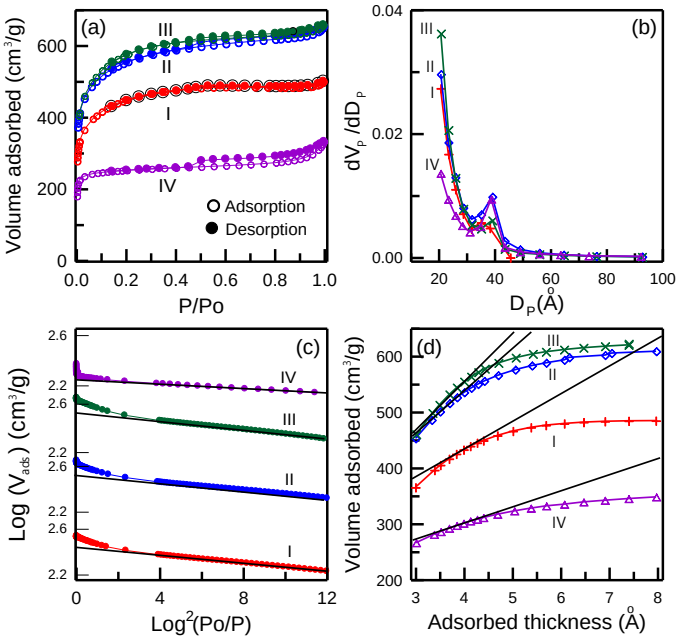

Fig. 5. (a) Adsorption-desorption isotherm, (b) differential pore size distribution, (c) DR-plot, and (d) *t*-plot of samples for two-stage activation at temperatures of 700 to 1000 °C (I 700 °C, II 800 °C, III 900 °C, and IV 1000 °C; P/P_o is the relative pressure; D_p is the pore size)

Table 4. Analysis of Pore Characteristics with Various Activation Temperatures for Two-Stage Activation [a]

°C	S_{BET} (m^2/g)	V_t (cm^3/g)	DR-plot		t-plot			
			V_{DR} (cm^3/g)	V_{DR}/V_t (%)	S_{ext} (m^2/g)	S_{mic} (m^2/g)	$V_{t\text{-plot}}$ (cm^3/g)	$V_{t\text{-plot}}/V_t$ (%)
700	1553	0.759	0.391	51.52	709	844	0.385	50.72
800	1912	0.900	0.524	58.22	773	1139	0.519	57.67
900	2093	1.001	0.533	53.25	862	1131	0.512	51.15
1000	851	0.481	0.298	61.95	128	723	0.336	69.85

S_{BET} = BET surface area, V_t = total pore volume, V_{DR} = micropore volume by DR-plot method, S_{ext} = external surface area, $V_{t\text{-plot}}$ = micropore volume by *t*-plot method.
[a] Samples were impregnated with NaOH at impregnation ratio of 3 and pre-pyrolysis temperature of 500 °C.

Analysis of Physical Properties

Figure 6(a) shows the X-ray diffraction analysis of fused silica in the DRS sample, with a diffraction peak around $2\theta = 22.5°$. For all AC samples, there were no characteristic peaks present (Figs. 6(b) to 6(e)). To measure the amount of ash (mainly silica component) in the samples, weighed amounts of DRS and AC were placed in the sample pan and then inserted into a furnace. These samples were heated to 900 °C under air. The weight percentage concentration of ash in DRS and AC were about 15.2 and 0.1 wt%, respectively. These data agreed with the XRD observations. However, a broad peak around $2\theta = 25°$

was observed in the XRD pattern. This peak indicated that the carbon materials were in a disordered form of turbostratic structure (Iwashita *et al.* 2004).

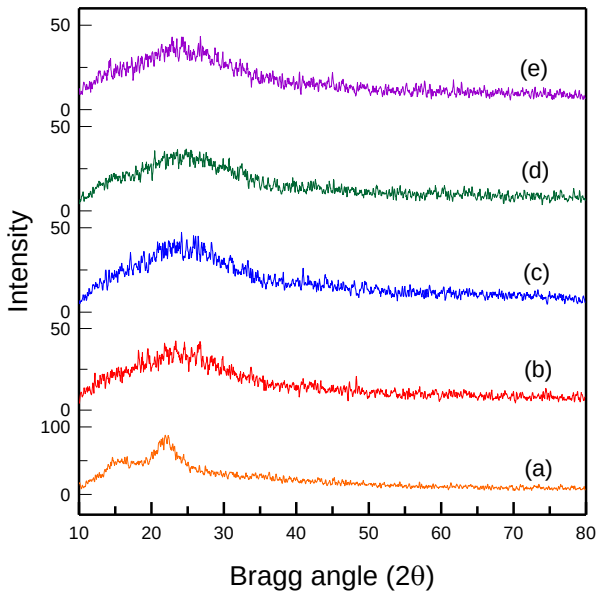

Fig. 6. X-ray diffractogram of samples. (a) DRS, (b through e) two-stage activation procedure and activation temperatures of 700 °C, 800 °C, 900 °C, and 1000 °C, respectively

The morphological features of the DRS and AC powders are shown in Fig. 7.

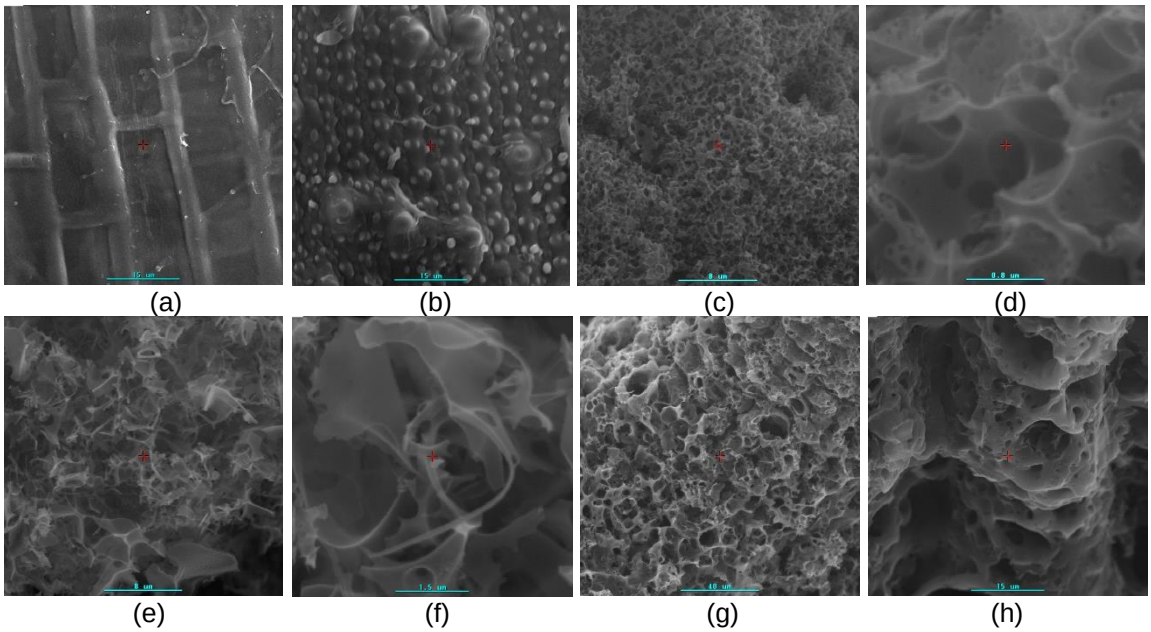

Fig. 7. Scanning electron micrographs of samples. (a) outer epidermis of rice straw (1500 X), (b) inner epidermis of rice straw (1500 X), (c)-(d) one-stage activation procedure at 700 °C and impregnation ratio of 1 (3000 X and 30000 X), (e)-(f) one-stage activation procedure at 700 °C and impregnation ratio of 3 (3000 X and 15000 X), (g)-(h) two-stage activation procedure at 900 °C and impregnation ratio of 3 (600 X and 1500 X)

Figure 7(a) shows the outer surface of the DRS, which was well-organized with a rectangular pattern. Inglesby *et al.* (2005) reported that the surface of untreated rice straw is covered with a thin layer of wax and is therefore quite smooth. Figure 7(b) shows the inner surface of DRS; it was corrugated and contained numbers of bulging tissues attached to the surface of the inner epidermis. Figures 7(c) and 7(d) show AC obtained from the one-stage activation procedure. The impregnation ratio of activating agent to DRS was 1. There were large pores of 0.5 to 1.0 μm distributed within the products, indicating carbon gasification on the external surface during activation (Hsu and Teng 2000). When the impregnation ratio was increased to 3 for one-stage activation, the fine and fiber shape products grew in large amounts within the AC tissue (Figs. 7(e) and 7(f)); the diameter was about 10 nm. Figures 7(g) and 7(h) show AC obtained from two-stage activation with an impregnation ratio of 3. Many large pores of 5 to 10 μm were formed on the surface of the carbonized specimen. Figure 7(h) clearly shows that there were many small pores distributed within the big pore walls. Comparing Figs. 7(c) and 7(g), the pore size in the one-stage activation procedure was obviously smaller than in the two-stage activation procedure. This observation agreed with the N_2-adsorption data (Figs. 3 and 4).

Analysis of Thermal Characteristics and Reaction Paths

The thermogravimetric analysis in Fig. 8(a) shows the remaining weight (W/W_o) for the one-stage activation procedure of DRS at an impregnation ratio of 2. The curves show an initial mass loss of up to a temperature of about 152 °C due to the elimination of physically adsorbed water in the samples. The mass loss occurring between 152 to 520 °C may be associated with the decomposition of organic materials. The temperature range of 520 to 850 °C corresponds to the activation process, which may be attributed to further reaction between the activating agent and the carbonaceous residue. Lillo-Rodenas *et al.* (2003) reported that the activation reaction between NaOH and C begins at around 570 °C, which was higher than in this study. Figure 8(a) also shows the derivative of weight (dW/dt) of the DRS activated in nitrogen (DTG curves). According to the peak temperature at the maximum instantaneous rate of thermal decomposition, DRS decomposed at 195 °C, 456 °C, and 575 °C.

The TGA plot of the DRS two-stage activation, obtained from an impregnation ratio of 2, is shown in Fig. 8(b). The mass loss of the pre-pyrolyzed DRS occurred in three temperature zones, namely 52 °C to 152 °C, 152 °C to 677 °C, and 677 °C to 877 °C. These results were similar to those of the one-stage activation. The similarity might be due to the use of the same carbon precursor and activating agent. The DTG curves show that the main temperature for the decomposition of pre-pyrolyzed DRS was 475 °C.

The activation reaction includes both rice straw and NaOH solid components at a high carbonization temperature, indicating that the activation path is complicated. The overall activation reaction is represented in Eqs. 2 or 3:

$$4NaOH + 2C \rightarrow 4Na + 2CO + 2H_2O \quad (2)$$

$$6NaOH + 2C \rightarrow 2Na + 3H_2 + 2Na_2CO_3 \quad (3)$$

At the surface of the DRS, NaOH is first decomposed to the Na_2O intermediate (Guo *et al.* 2003). Thus, the activation reaction can be divided into two groups. During the first group, Na_2O is generated through Eq. 4.

$$2NaOH \rightarrow Na_2O + H_2O \quad (4)$$

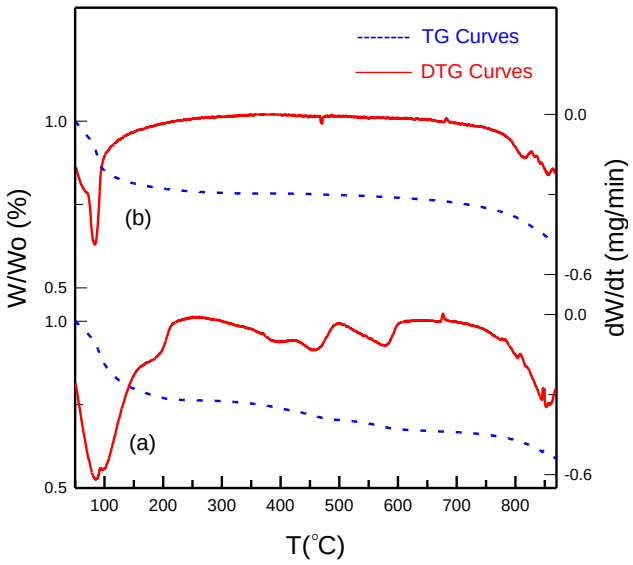

Fig. 8. TG and DTG thermograms of samples for (a) one-stage and (b) two-stage activation

In the second group, Na or Na_2CO_3 is generated *via* Eq. 5 or Eqs. 6 and 7. CO_2 is further decomposed as in Eq. 8.

$$2Na_2O + C \rightarrow 4Na + CO_2 \quad (5)$$

$$Na_2O + CO_2 \rightarrow Na_2CO_3 \quad (6)$$

$$2\ Na_2CO_3 + C \rightarrow 4Na + 3CO_2 \quad (7)$$

$$CO_2 + C \rightarrow 2CO \quad (8)$$

Reactions 5, 7, and 8 cause the carbon precursor to be removed as CO_2 or CO, and the surface area as well as the pore volume increases. At the initial stage of the reaction, the sample includes only a solid mixture of both carbon precursor and NaOH. Thus, the initial Na is produced (Eq. 5). After a certain period, Na_2O reacts with CO_2 to form Na_2CO_3 (Eq. 6). Na_2CO_3 subsequently reacts with carbon (Eq. 7). Hayashi *et al.* (2000) used lignin as a carbon source to prepare AC; when the Na_2CO_3 is the activating agent, the AC surface areas are far smaller compared with those of NaOH activation. Guo *et al.* (2003) reported that Na_2CO_3 is stable when the temperature was below 800 °C, which results in poor activation. In addition, according to the XRD analysis (Fig. 6), there was no Na_2CO_3 peak in the product. Thus, the overall activation reaction most likely occurred by Eq. 2. A few portions of the reaction also possibly proceeded by Eq. 3.

As mentioned earlier, rice straw has high ash content (mainly silica). The silica may obstruct the evolution of pore structures, which reduces the specific surface area and pore volume. However, the XRD analysis (Fig. 6) showed that the ash content disappeared after activation, which indicates that NaOH reacted with silica to synthesize sodium silicate (Na_2SiO_3). Na_2SiO_3 is soluble in water and can be removed by an adequate water-washing procedure (Liou and Yang 2011). The overall reaction for Na_2SiO_3 formation is as follows:

$$2NaOH + SiO_2 \rightarrow Na_2SiO_3 + H_2O \quad (9)$$

The silica in the interior tissue of rice straw disappeared through Eq. 9, and new pore structures were simultaneously formed. Thus, it was concluded that NaOH plays a dual role as an activating agent and as a cleaner to remove the ash.

CONCLUSIONS

1. Two-stage activation produced a higher surface area and iodine adsorption capacity than the one-stage activation procedure.
2. Pre-pyrolysis of rice straw effectively promotes mesoporous volumes.
3. The ash in the rice straw is removed through a reaction with the alkali activating agent. The reaction promotes pore formation.
4. The preparation of ACs from rice straw is beneficial to the recycling of agricultural wastes.

ACKNOWLEDGMENTS

The authors thank the Ministry of Science and Technology of Taiwan for its financial support under Project no. NSC 99–2221–E–131–018.

REFERENCES CITED

Basta, A. H., Fierro, V., El-Saied, H., and Celzard, A. (2011). "Effect of deashing rice straws on their derived activated carbons produced by phosphoric acid activation," *Biomass Bioenerg.* 35, 1954-1959. DOI: 10.1016/j.biombioe.2011.01.043

Chuah, T. G., Jumasiah, A., Azni, I., Katayon, S., and Choong, S. Y. T. (2005). "Rice husk as a potentially low-cost biosorbent for heavy metal and dye removal: An overview," *Desalination* 175, 305–316. DOI: 10.1016/j.desal.2004.10.014

El-Naggar, A. H., Alzhrani, A. K. R., Ahmad, M., Usman, A. R. A., Mohan, D., Ok, Y. S., and Al-Wabel, M. I. (2016). "Preparation of activated and non-activated carbon from *Conocarpus* pruning waste as low-cost adsorbent for removal of heavy metal ions from aqueous solution," *BioResources* 11(1), 1092-1107. DOI: 10.15376/biores.11.1.1092-1107

Guo, Y., Yu, K., Wang, Z., and Xu, H. (2003). "Effects of activation conditions on preparation of porous carbon from rice husk," *Carbon* 41, 1645-1648. DOI: 10.1016 /S0008-6223(03)00084-8

Hayashi, J., Kazehaya, A., Muroyama, K., and Watkinson, A. P. (2000). "Preparation of activated carbon from lignin by chemical activation," *Carbon* 38, 1873-1878.

Hsu, L. Y., and Teng, H. (2000). "Influence of different chemical reagents on the preparation of activated carbons from bituminous coal," *Fuel Process. Technol.* 64, 155-166.

Hu, Z., and Srinivasan, M. P. (1999). "Preparation of high-surface-area activated carbons from coconut shell," *Microporous Mesoporous Mat.* 27, 11-18.

Inglesby, M. K., Gray, G. M., Wood, M. F., Gregovski, K. S., Robertson, R. G., and Sabellano, G. P. (2005). "Surface characterization of untreated and solvent-extracted rice straw," *Colloid Surf. B* 43, 83-94. DOI: 10.1016/j.colsurfb.2005.03.014

Iwashita, N., Park, C. R., Fujimoto, H., Shiraishi, M., and Inagaki, M. (2004). "Specification for a standard procedure of X-ray diffraction measurements on carbon materials," *Carbon* 42, 701 -714. DOI: 10.1016/j.carbon.2004.02.008

Jain, A., Balasubramanian, R., and Srinivasan, M. P. (2015). "Production of high surface area mesoporous activated carbons from waste biomass using hydrogen peroxide-mediated hydrothermal treatment for adsorption applications," *Chem. Eng. J.* 273, 622-629. DOI: 10.1016/j.cej.2015.03.111

Kılıç, M., Apaydın-Varol, E., and Pütün, A. E. (2012). "Preparation and surface characterization of activated carbons from *Euphorbia rigida* by chemical activation with $ZnCl_2$, K_2CO_3, NaOH and H_3PO_4," *App. Surf. Sci.* 261, 247-254. DOI: 10.1016/j.apsusc.2012.07.155

Kim, C., and Pui, Y. H. (2015). "Experimental study on the filtration efficiency of activated carbons for 3–30 nm particles," *Carbon* 93, 226-229. DOI: 10.1016/j.carbon.2015.05.048

Lépinay, M., Broussous, L., Licitra, C., Bertin, F., Rouessac, V., Ayral, A., and Coasne, B. (2015). "Probing the microporosity of low-k organosilica films: MP and t-plot methods applied to ellipsometric porosimetry data," *Microporous Mesoporous Mat.* 217, 119-124. DOI: 10.1016/j.micromeso.2015.05.050

Lillo-Rodenas, M. A., Cazorla-Amoros, D., and Linares-Solano, A. (2003). "Understanding chemical reactions between carbons and naoh and koh: an insight into the chemical activation mechanism," *Carbon* 41, 267-275. DOI: 10.1016/S0008-6223(02)00279-8

Liou, T. H. (2010). "Development of mesoporous structure and high adsorption capacity of biomass-based activated carbon by phosphoric acid and zinc chloride activation," *Chem. Eng. J.* 158, 129-142. DOI: 10.1016/j.cej.2009.12.016

Liou, T. H., and Lai, B. C. (2012). "Utilization of e-waste as a silica source for the synthesis of the catalyst support MCM-48 and highly enhanced photocatalytic activity of supported titania nanoparticles," *Appl. Catal. B-Environ.* 115–116, 138-148. DOI: 10.1016/j.apcatb.2011.12.020

Liou, T. H., and Wu, S. J. (2009). "Characteristics of microporous/mesoporous carbons prepared from rice husk under base- and acid-treated conditions," *J. Hazard. Mater.* 171, 693-703. DOI: 10.1016/j.jhazmat.2009.06.056

Liou, T. H., and Yang, C. C. (2011). "Synthesis and surface characteristics of nanosilica produced from alkali-extracted rice husk ash," *Mater. Sci. Eng. B-Adv.* 176, 521-529. DOI: 10.1016/j.mseb.2011.01.007

Liu, B., Wang, W., Wang, N., and Au, C. T. (2014). "Preparation of activated carbon with high surface area for high-capacity methane storage," *J. Energy Chem.* 23, 662-668. DOI: 10.1016/S2095-4956(14)60198-4

Martins, A. C., Pezoti, O., Cazetta, A. L., Bedin, K. C., Yamazaki, D. A. S., Bandoch, G. F. G., Asefa, T., Visentainer, J. V., and Almeida, V. C. (2015). "Removal of tetracycline by NaOH-activated carbon produced from macadamia nut shells: Kinetic and equilibrium studies," *Chem. Eng. J.* 260, 291-299. DOI: 10.1016/j.cej.2014.09.017

Passe-Coutrin, N., Altenor, S., Cossement, D., Jean-Marius, C., and Gaspard, S. (2008). "Comparison of parameters calculated from the BET and Freundlich isotherms obtained by nitrogen adsorption on activated carbons: A new method for calculating the specific surface area," *Microporous Mesoporous Mat.* 111, 517-522. DOI: 10.1016/j.micromeso.2007.08.032

Pezoti, O., Cazetta, A. L., Bedin, K. C., Souza, L. S., Martins, A. C., Silva, T. L., Júnior, O. O. S., Visentainer, J. V., and Almeida, V. C. (2016). "NaOH-activated carbon of high surface area produced from guava seeds as a high-efficiency adsorbent for amoxicillin removal: Kinetic, isotherm and thermodynamic studies," *Chem. Eng. J.* 288, 778-788. DOI: 10.1016/j.cej.2015.12.042

Putum, A. E., Apaydin, E., and Putun, E. (2004). "Rice straw as a bio-oil source via pyrolysis and steam pyrolysis," *Energy* 29, 2171-2180. DOI: 10.1016/j.energy.2004.03.020

Scherdel, C., Reichenauer, G., and Wiener, M. (2010). "Relationship between pore volumes and surface areas derived from the evaluation of N_2-sorption data by DR-, BET- and t-plot," *Microporous Mesoporous Mat.* 132, 572-575. DOI: 10.1016/j.micromeso.2010.03.034

Sethia, G., and Sayari, A. (2015). "Comprehensive study of ultra-microporous nitrogen-doped activated carbon for CO_2 capture," *Carbon* 93, 68-80. DOI: 10.1016/j.carbon.2015.05.017

Tsai, W. T., Lee, M. K., and Chang, Y. M. (2006). "Fast pyrolysis of rice straw, sugarcane bagasse and coconut shell in an induction-heating reactor," *J. Anal. Appl. Pyrol.* 76, 230-237. DOI: 10.1016/j.jaap.2005.11.007

Tseng, R. L. (2006). "Mesopore control of high surface area NaOH-activated carbon," *J. Colloid Interface Sci.* 303, 494-502. DOI: 10.1016/j.jcis.2006.08.024

Vilaplana-Ortego, E., Lillo-Ródenas, M. A., Alcañiz-Monge, J., Cazorla-Amorós, D., and Linares-Solano, A. (2009). "Isotropic petroleum pitch as a carbon precursor for the preparation of activated carbons by KOH activation," *Carbon* 47, 2141-2142. DOI: 10.1016/j.carbon.2009.04.020

Yang, J., Yu, M., and Chen, W. (2015). "Adsorption of hexavalent chromium from aqueous solution by activated carbon prepared from longan seed: Kinetics, equilibrium and thermodynamics," *J. Ind. Eng. Chem.* 21, 414-422. DOI: 10.1016/j.jiec.2014.02.054

Zabaniotou, A., Stavropoulos, G., and Skoulou, V. (2008). "Activated carbon from olive kernels in a two-stage process: Industrial improvement," *Bioresour. Technol.* 99, 320-326. DOI: 10.1016/j.biortech.2006.12.020

Article submitted: December 20, 2015; Peer review completed: March 17, 2016;
Revisions accepted: May 18, 2016; Published: May 25, 2016.
DOI: 10.15376/biores.11.3.6110-6124